Economic Geology
Vol. 95, 2000, pp. 313–326

Bulk Rock and Melt Inclusion Geochemistry of Bolivian Tin Porphyry Systems

ANDREAS DIETRICH, BERND LEHMANN,†

Technische Universität Clausthal, Institut für Mineralogie und Mineralische Rohstoffe, 38678 Clausthal-Zellerfeld, Germany

AND ALEX WALLIANOS

Max-Planck-Institut für Kernphysik, 69029 Heidelberg, Germany

Abstract

The Miocene tin porphyry systems of Llallagua, Chorolque, and Cerro Rico have a moderately fractionated rhyodacite to dacite bulk rock composition. Ta, Zr, and TiO_2 concentrations are close to average upper crustal values. Hydrothermal overprint is reflected by strong enrichment of B, Bi, and Sn (>100 times upper crust) and by moderate enrichment of Sb, Pb, Ag, As, Au, and W (10–100 times upper crust). Melt inclusions in quartz phenocrysts have been analyzed by electron and proton microprobe techniques. The melt inclusions are characterized by highly fractionated rhyolitic composition with strong depletion of compatible components (0.02–0.14 wt % TiO_2, 15–85 ppm Zr). The trace element pattern with strong enrichment of incompatible elements (5–17 ppm Ta, 7–85 ppm As, 35–643 ppm B, 20–194 ppm Cs, 13–623 ppm Li, and 5–43 ppm Sn) is similar to tin granite systems. The compositional gap between melt inclusion and bulk rock geochemistry and the large compositional variations of trace elements among melt inclusions cannot be explained by crystal-liquid fractionation in a closed system alone.

We propose a scenario of selective quartz crystallization in a compositionally zoned magma chamber ranging from intermediate to highly fractionated melt portions. Influx of primitive melt into the magma chamber is thought to have resulted in mixing and to have triggered volcanic activity that led to the intermediate degree of fractionation of the exposed tin porphyry systems. Unexposed tin granitic portions released magmatic vapor phases that followed the volcanic vents and resulted in hydrothermal alteration and mineralization. Supply of magma and metals from different portions of compositionally zoned magma chambers can explain the exceptional metallogenic association of Bolivian tin porphyry mineralization with only moderately fractionated igneous rocks. It is probably those portions of a general tin granite composition that are chemically linked to tin mineralization, whereas the exposed rhyodacitic stocks essentially provide the structural focusing for magmatic vapor phases from a deeper stratified magma reservoir.

Introduction and Geology

THE TIN porphyry deposits of Llallagua, Chorolque, and Cerro Rico form part of the central Andean tin belt in the Eastern Cordillera of Bolivia (Fig. 1). The tin belt extends from southern Peru to northern Argentina and is the easternmost metallogenic province of the central Andes (Ahlfeld, 1967; Turneaure, 1971). Tin porphyry mineralization is in small stocks and volcanic complexes of rhyodacitic composition, characterized by pervasive hydrothermal overprint, stockwork-like brecciation, and hydrothermal breccias (Sillitoe et al., 1975; Grant et al., 1980). Early stages of hydrothermal alteration are penetrative with tourmalinization, and with sericitic and propylitic alteration toward distal portions. Mineralization occurs both disseminated and in complex vein systems.

The historical production figures of the Llallagua deposit are estimated at between 0.5 and 1 Mt Sn (Ahlfeld and Schneider-Scherbina, 1964; Redwood and Rice, 1997), which makes Llallagua the largest tin mine of the western world. The bulk geochemical tin enrichment of the system (resources and geochemical dispersion) is on the order of 2 Mt Sn. The Cerro Rico de Potosí is the historically most important silver producer of the world and became an important tin mine in the early twentieth century. The cumulated Ag production is estimated between 30,000 and 60,000 t Ag (Zartman and Cunningham, 1995).

†Corresponding author: email, lehmann@min.tu-clausthal.de

There are two major epochs of tin mineralization in Bolivia. Tin-tungsten mineralization in association with granitic systems of the Cordillera Real in northern Bolivia is of Triassic age (McBride et al., 1983). Tertiary tin mineralization divides geographically into two groups. A northern group of Sn-W deposits of late Oligocene to lower Miocene ages includes the granitic plutons of Illimani, Quimsa Cruz, and Santa Vera Cruz, and subvolcanic stocks such as the Llallagua deposit. An upper Miocene group of Sn-W-Bi-Ag-Pb-Zn mineralization is associated with very shallow volcanic systems and occurs in the southern part of the eastern Cordillera, comprising the Cerro Rico and the deposits of the Quechisla mining district with Chorolque, Tasna, and Chocaya (Sillitoe et al., 1975; Grant et al., 1977, 1980).

This study is based on results of a geochemical reconnaissance project. Although some of the tin porphyries are world-class deposits, little geochemical work has been carried out to date. Bulk rock geochemistry by X-ray fluorescence (XRF), inductively coupled plasma-mass spectrometry (ICP-MS), atomic absorption spectrometry (AAS), instrumental neutron activation analysis (INAA), and direct coupled plasma spectrometry (DCP) provides a comprehensive data set of the major and trace element spectrum. Additional microanalytical work on quartz-hosted melt inclusions by electron microprobe analysis (EMPA) and proton-induced X-ray emission analysis (PIXE) allows insight into the magmatic and transitional magmatic-hydrothermal history of the tin porphyry systems.

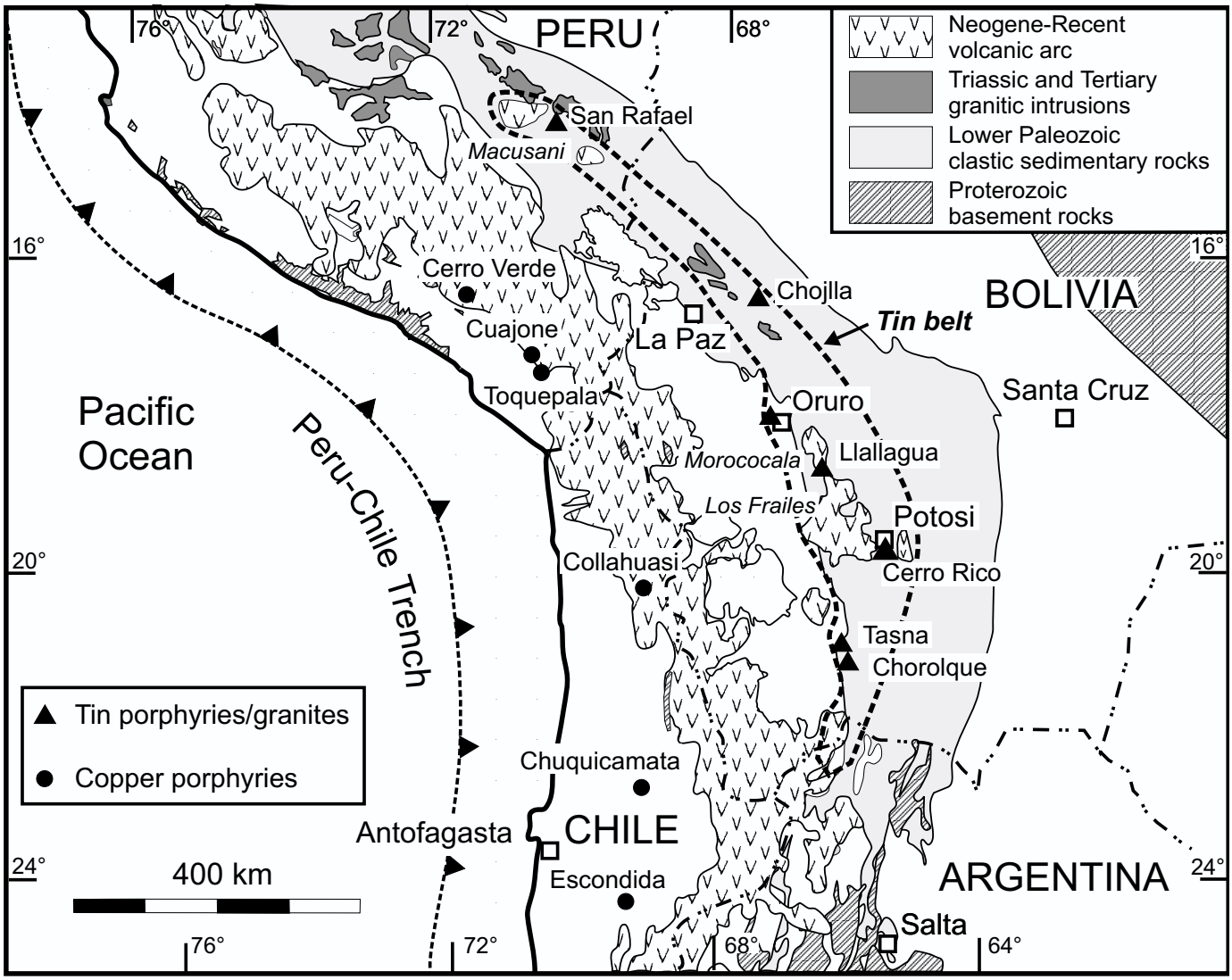

FIG. 1. Geologic setting of the Andean tin belt and location of major ore deposits.

Llallagua

The tin porphyry of Llallagua, also known as Siglo XX, Catavi, and Uncía, is situated about 80 km southeast of Oruro. The hydrothermal system and mineralization is centered on the 1,700 × 1,000 m large Salvadora stock of lower Miocene age (K-Ar age of 20.6 ± 0.35 Ma; Grant et al., 1979), which intruded into a north-northwest–south-southeast-striking anticline of Silurian metasedimentary rocks (Ahlfeld, 1931; Samoyloff, 1934; Turneaure, 1935, 1960). The emplacement of the Salvadora stock was probably controlled by a set of north-northwest–south-southeast-striking dextral strike-slip faults. The subvolcanic stock is built up of four lithologies: (1) a rhyodacitic core, grading out into (2) a rhyodacitic igneous breccia near the contacts; (3) crosscutting rhyodacitic dikes; and (4) hydrothermal breccias. The subvolcanic and adjacent sedimentary rocks are strongly hydrothermally altered. Quartz-sericite alteration predominates near the surface. The degree of tourmalinization increases with depth. Sericitic to propylitic alteration is developed in distal parts of the system (Sillitoe et al., 1975; Grant et al., 1977, 1980).

The rhyodacitic core contains fine- to medium-grained phenocrysts of quartz, feldspars, and biotite (both feldspars and biotite are altered to fine-grained quartz-sericite-tourmaline aggregates), set in a fine-grained matrix. Phenocrysts comprise about 40 to 50 vol percent of the rock and are commonly broken into fine-grained fragments. The phenocryst ratio is approximately 35 vol percent quartz, 50 vol percent feldspars, and 15 vol percent biotite. Accessory constituents are zircon, apatite, and leucoxene. Small amounts of igneous clasts with subvolcanic but petrographically similar characteristics can be recognized locally in less-altered portions of the stock.

The rhyodacitic breccia is best developed close to the contact with the sedimentary host rock, and grades continuously into the rhyodacitic core. The breccia has greater than 20 vol percent of sedimentary clasts. The clasts are angular to partially subrounded, with sizes from a few millimeters to 20 cm. The stock is crosscut by two east-west-striking rhyodacitic

dikes characterized by coarse-grained to megacrystic, hypidiomorphic to idiomorphic sanidine crystals (20 vol %), and fine- to medium-grained phenocrysts of plagioclase, quartz, and biotite embedded in a very fine grained groundmass.

The hydrothermal breccias occur as dikelike to pipelike bodies, having a tourmaline and silica-cemented matrix of crushed rock. Angular to subrounded clasts of both sedimentary and volcanic rocks make up about 40 vol percent of the rock.

Tin mineralization occurs both as disseminated cassiterite and in quartz-tourmaline-cassiterite-sulfide veins and veinlets. The veins strike between 20° and 40° north and dip steeply toward the northwest or southeast. Formation of veins as synthetic branch faults was in conjunction with dextral movements along the north-south-striking Diaz-Stanton fault system, which crosscuts the stock.

Chorolque

The tin porphyry system of Chorolque is located about 30 km east of Atocha, a railway station and village between Uyuni and Tupiza in the southern Bolivian tin belt. The volcanic complex consists of a volcanic vent, about 1 km in diameter, and surrounding crystal- and pumice-rich ash flow tuffs. The vent and tuffs crosscut and overlie folded siliciclastic Ordovician country rocks. The Chorolque volcanic complex is regarded as a volcanic center to the nearby Atocha tuff units, which therefore represent the unaltered facies of the Chorolque ash flow tuffs. Both the Chorolque and Atocha tuffs to the west were deposited onto a palaeosurface with westerly dip and are separated by a 3-km-wide erosional gap. Whole rock analyses of the altered Chorolque tuffs yield K-Ar ages of 16.2 ± 0.3 Ma and 18.4 ± 0.7 Ma, whereas biotite from the Atocha tuffs gave a K-Ar age of 16.8 ± 0.3 Ma (Grant et al., 1979).

A concentric alteration pattern is developed around the volcanic vent that channeled hydrothermal fluids into the overlying volcanic rocks. The strongly tourmalinized center within and above the volcanic vent grades out into a ring of sericitization with stockworklike brecciation of the rock and porphyry-style disseminated and veinlet mineralization of sulfides and cassiterite. More distal areas were affected by propylitic alteration. Silicification accompanies all alteration styles, but its intensity decreases from the volcanic vent toward distal parts of the system (Grant et al., 1977, 1980).

The ash flow tuffs are composed of about 50 vol percent phenocrysts and their broken fragments, set in a dense groundmass. Pumice lapilli are centimeters to decimeters in diameter, and make up about 30 vol percent of the rock. Slight to moderate compaction of the pumices indicates partial welding of the tuffs. The phenocryst assemblage consists of fine- to medium-grained crystals of quartz (15–20 vol %), feldspars (20–25 vol %), biotite (5–10 vol %), rare hornblende relics, and accessory zircon, apatite, and leucoxene. Samples of the unaltered Atocha tuffs show hypidiomorphic plagioclase with normal zonation (~An_{40}–An_{55}) and sometimes clear breaks from Ca-rich cores to slightly oscillating rims. Broken fragments of sanidine make up about 5 vol percent of the rock. The Atocha tuffs contain centimeter-scale, large spherical biotite-rich inclusions of andesitic composition. Xenomorphic to hypidiomorphic biotite (25 vol %) and hypidiomorphic plagioclase (50 vol %) are enclosed poikilitically by xenomorphic orthoclase and quartz (25 vol %). The andesitic inclusions of the Atocha tuffs have porous texture, are partly filled with leucoxene, and show a slight decrease in average grain size from core to rim. These inclusions may be restites, but they also have some characteristic features of quenched andesitic inclusions, which are generated by mixture of primitive and felsic melts (Stimac and Pearce, 1992).

The tourmalinized core of the Chorolque system has no significant petrographic difference to the surrounding ash flow tuffs apart from hydrothermal overprint, and it is interpreted as a pyroclastic vent. The amounts of quartz phenocrysts and pseudomorphs after feldspars and biotite appear to be the same both within and outside the vent.

The main mineralization occurs in east-west-striking and steeply dipping (70°) veins. Most veins are located in the tourmaline-rich center of the system, although some extend about 1,000 m out into the country rock. Vein mineralization displays a temperature zonation with quartz-tourmaline-cassiterite in the center, grading out into quartz-wolframite-pyrite and Bi-Ag-Pb-Cu-Zn mineralization in distal portions (Sugaki et al., 1985).

Cerro Rico de Potosí

The Cerro Rico is the landmark of the historical mining town of Potosí in the southern, Eastern Cordillera of Bolivia. The mushroom-shaped dome has a U-Pb age of 13.8 ± 0.2 Ma (Zartman and Cunningham, 1995) and intruded an Ordovician sedimentary sequence and overlying Miocene sediments and tuffs. Emplacement of the dome was controlled either by a ring fault of the lower Miocene Karikari resurgent caldera or by a tensile bridge structure between north-northwest-striking en echelon faults generated by dextral shear along the Carma fault (Francis et al., 1981; Steele, 1996).

The rock consists of 40 to 50 vol percent of phenocrysts of corroded quartz and altered relics of plagioclase, sanidine, and biotite set in a strongly altered, dense groundmass. Accessory phases other than zircon were affected by hydrothermal alteration. A predominantly vertical alteration zonation has resulted in a high-sulfidation lithocap with silicification (vuggy silica) and quartz-dickite alteration with disseminated silver mineralization at the summit, underlain by predominantly sericitic alteration which grades into tourmalinization at deepest levels. Prominent polymetallic veins strike northeast-southwest to north-south and crosscut the stock and surrounding country rock. Vein mineralization consists of pyrite, galena, sphalerite, complex Ag-sulfides, wolframite, and cassiterite with quartz, tourmaline, kaolinite, alunite, sericite, and siderite as gangue minerals (Turneaure, 1960; Rivas and Carrasco, 1968; Sillitoe et al., 1975, 1998; Steele, 1996). Sulfur isotopes suggest a magmatic origin of sulfur and point to reduced ore-bearing hydrothermal fluids (G.B. Steele, pers. commun., 1997; Sillitoe et al., 1998).

The detailed geochronological study of Cunningham et al. (1996) showed that intrusion was immediately followed by hydrothermal alteration and mineralization. U-Pb ages of magmatic zircon (13.8 ± 0.2 Ma) overlap with $^{40}Ar/^{39}Ar$ ages (13.76 ± 0.1 Ma) of hydrothermal sericite. A second stage of alteration (and probably of mineralization) has been detected at between 11 and 10 Ma.

Bulk Rock Geochemistry

Rock samples of 1 to 2 kg each from Llallagua (n = 21), Chorolque (n = 18), and Cerro Rico (n = 11) were selected both from surface and underground mine exposures. Some additional reconnaissance samples from the tin porphyry of Oruro (n = 8) are surface samples. All samples of the tin porphyry systems have pervasive hydrothermal overprint (quartz-sericite ± tourmaline) and are from disseminated and stockwork mineralization. Vein mineralization has not been sampled. Bulk rock geochemistry was carried out by XRF, ICP-MS, INAA (n = 58), AAS, and DCP (n = 45). The chemical data are compiled in Table 1.

The classic Zr/TiO_2 vs. SiO_2 discrimination diagram of Winchester and Floyd (1977) classifies the tin porphyry samples as rhyodacitic to dacitic rocks, with some scatter toward the rhyolitic field attributed to hydrothermal overprint (Fig. 2). The unaltered Atocha tuffs near Chorolque plot in the rhyodacite-dacite field and their biotite-rich inclusions plot at the dacite-andesite boundary.

Immobile element data define a generally moderate degree of fractionation with mean values between 0.57 and 0.67 wt percent TiO_2, 135 and 294 ppm Zr, and 1.5 and 3.4 ppm Ta (Table 1). Whole rock abundances of immobile elements are between average bulk and upper continental crust, with element patterns typical of intermediate, calc-alkaline magmatic rocks.

Very high average boron concentrations on the order of up to 400 times upper crust (Chorolque) resulted from intense tourmalinization, a typical feature of all Bolivian tin systems. Fluorine is only enriched by a factor of about two times upper crust. The hydrothermal overprint has strongly increased Bi and Sn abundances (>100 × upper crust). Moderate enrichment by a factor of 10 to 100 times upper crust is seen for Sb, Pb, Ag, As, Au, and W. The Cerro Rico has average concentrations greater than 100 times upper crust for Sb and Ag. Cu and Zn are near upper crustal values.

The rare earth element (REE) distribution patterns of the Llallagua, Chorolque, and Oruro tin porphyries are relatively inconspicious and show moderate La/Lu fractionation and weak negative Eu anomalies (Fig. 3). The samples of the Cerro Rico display a steeper REE distribution with lower heavy REE contents presumably due to a residual garnet-bearing source or to garnet fractionation. The Cerro Rico forms part of the Los Frailes-Karikari volcanic field. The ash flow tuffs and lavas of the Miocene Karikari volcanic field contain garnet as an accessory constituent (Wolf, 1973; Francis et al., 1981; Schneider, 1985). Some samples of the Cerro Rico and Oruro systems show either no or positive Eu anomalies. However, positive Eu anomalies are not typical features of the bulk systems and are attributed to hydrothermal REE redistribution (see also Cunningham et al., 1996).

Reconnaissance isotope geochemistry (Table 2) gave ε_{Nd} values of –9 for hydrothermally altered bulk rock samples of Llallagua, ε_{Nd} of –7 to –6 for Chorolque, and ε_{Nd} = –5 for the Cerro Rico. Depleted mantle model ages are between 781 and 1148 Ma. The neodymium isotope data of the tin porphyries are within the compositional range of Tertiary igneous rocks of the tin belt. The volcanic rocks of the Karikari-Los Frailes field have ε_{Nd} of –5 to –6 (Schneider, 1985), the Quimsa Cruz granite (Mina Viloco) has ε_{Nd} of –10.6 and –4.7 (Miller and Harris, 1989), and the strongly peraluminous Macusani tuffs, with inferred metapelitic source, have ε_{Nd} around –9 (Pichavant et al., 1988). The Proterozoic basement of the Altiplano, exposed in the Tertiary Azurita conglomerate and in drillholes of petroleum exploration, has ε_{Nd} between –11 and –14 (Aitcheson and Moorbath, 1992, unpubl. data). The lower Paleozoic sedimentary sequence of the Eastern Cordillera has ε_{Nd} values between –8 and –12 (Miller and Harris, 1989; Basu et al., 1990). Our Nd data on the tin porphyry systems point to a dominantly middle to upper crustal origin, with, however, some values requiring mantle input.

Melt Inclusions

Petrography of melt inclusions

Melt inclusions are entrapped silicate melt phases in phenocrysts (Roedder, 1979, 1984; Lowenstern, 1995). Melt inclusions hosted only in quartz phenocrysts were investigated in this study, due to hydrothermal overprint of all other phenocrystic minerals. The inclusion occurrences vary from random to sievelike distributions within quartz phenocrysts. In some quartz of the Chorolque system, melt inclusions also are entrapped along roundish crystal growth lines. The strong magmatic corrosion and common fragmentation of phenocrysts make a safe correlation of the position of melt inclusions with the growth history of their host crystals impossible. There is no evidence for multiple generations of quartz phenocrysts, and nearly all corroded crystals and fragments contain melt inclusions.

The melt inclusions of Llallagua have roundish shapes, with sizes up to 60 μm. The mostly devitrified and cryptocrystalline, dark-colored melt inclusions were routinely homogenized (remelted) under atmospheric conditions in a tube

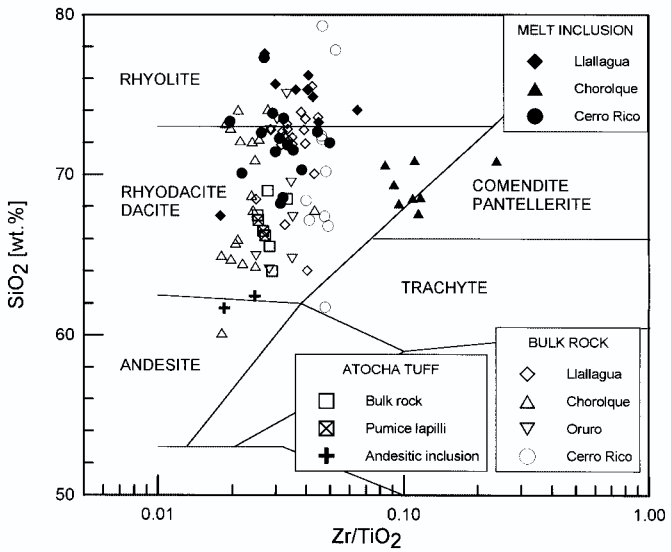

FIG. 2. Zr/TiO_2 vs. SiO_2 discrimination diagram for bulk rock and melt inclusion data of Bolivian tin porphyries and for samples of the unaltered Atocha tuff, sensu Winchester and Floyd (1977). Note that melt inclusion data represent fractionated melt fractions, not bulk rock compositions; individual data in Dietrich (1999).

TABLE 1. Bulk Rock Geochemistry of the Bolivian Tin Porphyry Systems

			Llallagua				Chorolque				Cerro Rico				Oruro			
			Mean	±1σ	Max	Min	Mean	±1σ	Max	Min	Mean	±1σ	Max	Min	Mean	±1σ	Max	Min
SiO_2	wt %	XRF	71.8	2.5	75.5	64.0	68.7	4.0	74.1	60.1	72.5	8.4	94.5	61.8	69.0	4.1	75.0	64.1
TiO_2	wt %	XRF	0.58	0.05	0.71	0.51	0.57	0.12	0.85	0.45	0.64	0.10	0.83	0.46	0.67	0.06	0.78	0.59
Al_2O_3	wt %	XRF	15.3	0.9	16.5	12.7	14.8	1.6	18.3	10.7	12.2	4.0	15.4	1.1	14.1	1.5	15.6	11.4
Σ FeO	wt %	XRF	2.46	1.46	7.50	0.81	4.69	2.87	10.34	1.21	3.62	2.30	7.86	0.35	3.25	1.00	5.16	1.81
MnO	wt %	XRF	0.02	0.03	0.14	0.01	0.02	0.03	0.11	0.01	0.02	0.01	0.03	0.01	0.15	0.28	0.90	0.02
MgO	wt %	XRF	1.01	0.33	1.74	0.50	1.39	0.67	2.91	0.38	0.28	0.18	0.60	0.02	0.87	0.53	2.12	0.45
CaO	wt %	XRF	0.10	0.05	0.23	0.04	0.14	0.07	0.27	0.04	0.11	0.05	0.21	0.06	0.87	0.97	2.82	0.07
Na_2O	wt %	XRF	0.30	0.19	0.64	0.02	0.46	0.42	1.84	0.01	0.58	1.17	3.19	0.01	1.25	1.37	3.71	0.02
K_2O	wt %	XRF	3.50	1.62	7.20	0.29	2.65	2.38	7.56	0.08	2.46	1.47	3.70	0.07	4.02	1.13	5.67	1.95
P_2O_5	wt %	XRF	0.14	0.07	0.27	0.03	0.11	0.06	0.18	0.03	0.35	0.13	0.51	0.06	0.14	0.07	0.24	0.05
LOI	wt %	XRF	2.89	0.94	6.19	1.49	3.47	2.21	10.39	1.49	4.87	1.52	6.17	0.62	4.11	1.34	5.48	1.15
SUM	wt %	XRF	98.3	0.9	99.7	95.7	97.5	2.3	101.0	93.0	97.8	1.3	99.0	93.9	98.8	1.1	99.9	96.0
B	ppm	DCP	3,503	2,504	7,994	87	5,918	5,085	12,871	106	440	482	1,371	45	3,121	4,430	11,634	177
F	ppm	ISE	1,245	455	2,286	276	732	672	2,479	148	2,656	1,119	4,310	998	966	366	1,498	572
Cr	ppm	XRF	46	24	128	14	62	29	167	42	26	10	39	10	41	28	107	22
Cu	ppm	AAS	127	251	943	3	31	55	192	2	22	30	87	2	6	3	10	2
Zn	ppm	AAS	214	344	1,257	6	30	42	143	3	214	282	733	8	547	1,045	2,637	5
As	ppm	INAA	55	60	245	2	100	176	772	3	98	57	186	13	27	31	87	1
Rb	ppm	ICP-MS	255	112	470	16	161	153	456	2	235	152	472	4	206	70	321	94
Sr	ppm	ICP-MS	48	44	161	11	72	80	271	3	985	925	2,478	51	130	74	254	56
Zr	ppm	ICP-MS	206	40	317	140	135	46	251	85	294	48	364	218	209	19	232	178
Mo	ppm	INAA	1.8	0.8	3.0	1.0	2.1	0.8	3.0	1.0	4.8	1.6	8.0	3.0	2.0	1.1	4.0	1.0
Ag	ppm	AAS	1.9	1.7	5.7	0.2	1.2	2.3	10.2	0.1	8.6	10.2	32.2	0.2	3.4	4.4	11.5	0.2
Sn	ppm	AAS	570	853	3,443	60	170	162	659	18	566	637	2,051	44	58	58	148	7
Sb	ppm	INAA	15	13	54	3	18	25	107	3	68	67	250	8	45	61	176	1
Cs	ppm	ICP-MS	20	26	127	5	7	8	29	1	14	9	32	2	19	12	42	3
Ba	ppm	ICP-MS	535	512	1,956	77	229	325	1,108	11	467	163	696	193	876	315	1,247	235
Hf	ppm	ICP-MS	5.4	1.0	8.2	3.7	3.9	1.2	6.7	2.5	6.8	1.1	8.4	5.2	5.7	0.5	6.3	5.0
Ta	ppm	INAA	1.6	0.2	1.9	1.1	1.5	0.2	2.0	1.1	3.4	0.6	4.6	2.4	1.5	0.2	1.8	1.2
W	ppm	INAA	20	16	61	1	24	29	132	1	9	5	19	4	5	4	14	2
Au	ppb	INAA	38	47	232	8	54	67	290	11	24	9	37	13	41	20	85	17
Pb	ppm	ICP-MS	782	2,257	8,094	4	29	33	129	4	869	1,059	2,677	5	291	532	1,687	24
Bi	ppm	AAS	25	34	109	2	28	36	112	4	3	2	5	1	<1	–	<1	<1
Th	ppm	ICP-MS	14	3	24	9	13	5	23	4	20	6	26	3	15	1	17	14
U	ppm	ICP-MS	5	2	14	3	4	2	7	1	10	2	11	4	4	0	5	3

Analytical methods: X-ray fluorescence spectrometry (XRF), inductively coupled plasma-mass spectrometry (ICP-MS), instrumental neutron activation analysis (INAA), F-Potentiometry (ISE), atomic absorption spectrometry (AAS), direct coupled plasma spectrometry (DCP)

Number of samples: Llallagua (n = 21), Chorolque (n = 18), Oruro (n = 8), Cerro Rico (n = 11); from Dietrich, 1999

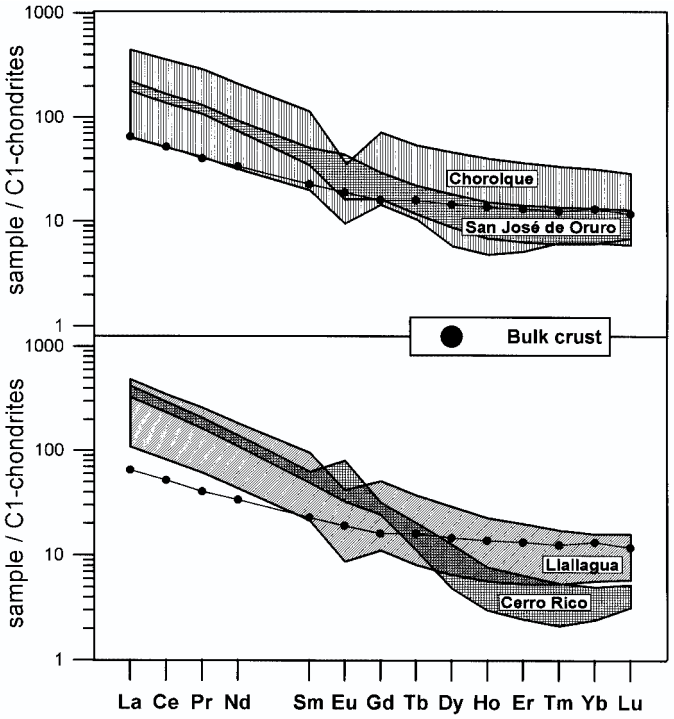

FIG. 3. Rare earth element distribution patterns of the tin porphyry systems of Llallagua (n = 21), Chorolque (n = 18), Oruro (n = 8), and Cerro Rico (n = 11; Dietrich, 1999); bulk crust data from Taylor and McLennan (1985).

oven (24 h, 800–1,000°C) prior to analysis. After homogenization and quenching, the melt inclusions consist of colorless glass with a vapor bubble of about 5 vol percent.

Quartz phenocrysts of the Chorolque and Cerro Rico deposits contain negative crystal-shaped melt inclusions with sizes up to 100 μm. The most well-developed inclusions show habits of hexagonal bipyramides without prism faces. Large shrinkage-vapor bubbles mostly share about 20 percent of the volume of the inclusions. The quartz phenocrysts of Cerro Rico enclose large amounts of fine apatite needles, and their ends are commonly surrounded by glass droplets. The Chorolque and Cerro Rico samples have not been artificially homogenized routinely because abundant melt inclusions are preserved as colorless glass.

Vapor bubbles of nonremelted melt inclusions are coated with microcrystalline aggregates of platy to flaky minerals. The element spectrum of Si, Al, Na, Mg, Cl, K, and Fe, detected by scanning electron microscope-energy dispersive X-ray analysis (SEM-EDX), suggests micas, feldspars, and chlorides.

Additionally, quartz phenocrysts enclose some negative crystal-shaped empty cavities, interpreted as primary, pure vapor inclusions, as well as melt inclusions with exceptionally large gas bubbles (>50 vol %). These inclusions have not been the target of microanalysis.

Microanalytical conditions

Microanalysis was done by electron (EMPA) and proton microprobes (PIXE; Tables 3, 4). Only melt inclusions with sizes greater than 20 μm were selected for geochemical analysis. Homogeneity of the melt inclusions was checked by backscattered electron (BSE) images, elemental scans, and mapping. We used a CAMECA SX100 electron microprobe at low energy operating conditions of 15 kV, 10 nA, and 10 μm beam. Na and K were measured during the first 20 s of each analysis to minimize alkali diffusion in hydrous glasses (Nielsen and Sigurdson, 1981; Morgan and London, 1996). Results of Na and K contents have not been corrected because there was no significant decrease of Na and K intensities during the first 30 s. Morgan and London (1996) found exponential decrease of Na intensities on water-rich glasses (~5 wt % H_2O) within 60 s, but water contents of our melt inclusions are significantly lower (<2 wt %). The reliability of analyses was controlled by the anhydrous MM3 obsidian glass standard (Nash, 1992).

Proton-induced X-ray emission (PIXE) analysis was done at the Heidelberg proton microprobe (Traxel et al., 1995) using incident protons at energies of 2.2 MeV, beam currents less than 100 pA, and counting times up to 20 h. Calibration is by pure elements and is checked by a number of international glass standards. Data reduction is by the GUPIX software (Maxwell et al., 1989, 1995), with adjustment for melt inclusion thickness by Fe concentration from EMPA. Limits of detection depend on individual matrix composition and are in the range of a few ppm to a few tens of ppm for most elements with atomic number higher than 20 (Ca; Wallianos, 1998).

Nuclear reaction analysis (NRA) for B and Li (Table 4) was carried out at the Saclay nuclear microprobe, Laboratoire Pierre Sue, France using an incident proton beam at 700 KeV and the nuclear reactions of $^{11}B(\rho,\alpha)^{8}Be$ and $^{7}Li(\rho,\alpha)^{4}He$. Limits of detection are 10 ppm B and 50 to 100 ppm Li. For analytical details see Mosbah et al. (1995), Rio et al. (1995), and Wallianos (1998).

TABLE 2. Neodymium Isotope Data of the Tin Porphyry Systems of Llallagua, Chorolque, and Cerro Rico

Sample	Locality	Material	Sm (ppm)	Nd (ppm)	$^{147}Sm/^{144}Nd$ [1]	$^{143}Nd/^{144}Nd$ [2]	Depleted source (Ma)	ε_{Nd} (T = 10 Ma)
L18b	Llallagua	Sanidine	10.805	10.521	0.6208	0.512117 ± 19		–10.7 ± 0.4
L18a	Llallagua	Bulk rock	10.212	63.408	0.0974	0.512163 ± 23	1148	–9.1 ± 0.5
L22	Llallagua	Bulk rock	9.221	59.366	0.0939	0.512158 ± 30	1121	–9.2 ± 0.6
C56	Chorolque	Bulk rock	9.636	67.909	0.0857	0.512278 ± 15	911	–6.9 ± 0.3
C64	Chorolque	Bulk rock	7.780	42.325	0.1111	0.512343 ± 26	1037	–5.7 ± 0.5
P94a	Cerro Rico	Bulk rock	9.787	74.683	0.0792	0.512357 ± 9	781	–5.3 ± 0.2

[1] Analytical error <0.3 percent (2 σ)
[2] 2 σ errors; depleted mantle source age calculated with ISOPLOT (Ludwig, 1993)

TABLE 3. Melt Inclusion Geochemistry

			Llallagua				Chorolque				Cerro Rico			
			Mean	± 1σ	Max	Min	Mean	± 1σ	Max	Min	Mean	± 1σ	Max	Min
SiO_2	EMPA	wt %	74.9	2.5	78.2	64.5	69.2	1.0	70.9	67.0	71.6	1.5	74.0	66.7
TiO_2	PIXE	wt %	0.09	0.02	0.12	0.06	0.06	0.01	0.08	0.03	0.08	0.02	0.14	0.05
Al_2O_3	EMPA	wt %	13.0	2.7	21.6	9.4	16.7	0.8	18.9	15.7	15.0	0.7	15.9	13.0
Σ FeO	EMPA	wt %	0.74	0.16	1.15	0.41	0.62	0.22	0.98	0.33	0.54	0.13	0.77	0.29
MnO	EMPA	wt %	0.06	0.03	0.16	<0.03	0.05	0.02	0.10	0.03	0.05	0.01	0.07	<0.03
MgO	EMPA	wt %	0.11	0.02	0.16	0.06	0.06	0.03	0.12	<0.01	0.04	0.04	0.14	<0.01
CaO	EMPA	wt %	0.61	0.20	1.06	0.24	1.44	0.46	2.64	0.79	0.52	0.25	1.56	0.16
Na_2O	EMPA	wt %	3.29	1.06	5.31	1.32	2.47	0.62	3.25	1.67	1.48	0.72	2.91	0.49
K_2O	EMPA	wt %	4.41	0.69	5.60	3.30	7.18	0.50	8.49	6.39	6.86	0.59	8.34	5.57
P_2O_5	PIXE	wt %	0.34	0.42	1.39	<0.13	0.05	0.01	0.06	<0.13	0.20	0.11	0.53	<0.19
F	EMPA	wt %	<0.06	0.02	0.09	<0.03			<0.03		0.07	0.03	0.18	<0.03
SUM	EMPA	wt %	96.9	2.6	102.4	92.9	98.1	1.8	101.0	95.2	97.0	1.4	99.2	92.7
S	PIXE	ppm	104	49	181	<40	72	8	80	<48	197	11	207	<43
Cl	PIXE	ppm	1,552	1,391	6,060	715	2,110	681	2,868	973	1,439	456	2,144	590
Zn	PIXE	ppm	43	11	64	29	19	7	25	4	31	17	57	7
As	PIXE	ppm	12	4	20	7	50	8	65	39	40	18	85	14
Br	PIXE	ppm	2	0.8	4	1	5	3	11	<1	2	1.1	4	<1
Rb	PIXE	ppm	274	65	387	176	314	39	386	270	463	83	637	292
Sr	PIXE	ppm	53	30	101	18	131	32	178	94	62	29	103	11
Zr	PIXE	ppm	38	21	77	17	66	12	85	47	27	8	36	15
Nb	PIXE	ppm	20	19	73	<5	15	3	20	11	26	5	32	14
Sn	PIXE	ppm	29	5	39	<13	33	7	40	<12	29	9	43	<10
Cs	PIXE	ppm	77	34	117	<14	30	1	31	29	102	50	194	20
Ba	PIXE	ppm	247	136	387	95	367	177	592	76	128	67	269	<38
Hf	PIXE	ppm	10	5	18	<4	10	4	18	<5	10	4	19	6
Ta	PIXE	ppm	8	1	10	<4	8	2	12	<5	9	4	17	<6
W	PIXE	ppm	20	15	47	<2	13	4	21	8	10	5	20	<3
Pb	PIXE	ppm	35	16	64	16	64	63	224	27	31	27	110	17
Th	PIXE	ppm	21	14	40	<6	28	12	43	<12	6	2	8	<3
U	PIXE	ppm	<LOD			<9	21	5	28	17	23	6	32	14

Electron microprobe analyses (EMPA): Llallagua, n = 30, Chorolque, n = 18, Cerro Rico, n = 33; PIXE analyses: Llallagua, n = 12, Chorolque, n = 7, Cerro Rico, n = 12; individual data in Dietrich (1999)

LOD = limits of detection

TABLE 4. B and Li Concentrations of Melt Inclusions from Nuclear Reaction Analysis (NRA) and Secondary-Ion Mass Spectrometry (SIMS) Analyses

	B		Li	
Sample	Method	ppm	Method	ppm
C36-4	NRA	233 ± 29	NRA	248 ± 71
P94b-2	NRA	162 ± 23	NRA	71 ± 42
P95-3	NRA	265 ± 34	NRA	189 ± 69
P97-3	NRA	643 ± 76	NRA	35 ± 35
P97-6	NRA	346 ± 46	SIMS	13 ± 5
P97-4	NRA	179 ± 28	SIMS	13 ± 5
L24a-3	NRA	35 ± 5	NRA	623 ± 80
L24a-2	NRA	105 ± 17	NRA	520 ± 122
P95-4	SIMS	71 ± 8	SIMS	106 ± 4
P97-2	SIMS	275 ± 19	SIMS	13 ± 5
P95-1	NRA	357 ± 64	NRA	264 ± 112
C44-2	NRA	275 ± 13		

Notes: L samples = Llallagua; C samples = Chorolque; P samples = Cerro Rico de Potosí

Additional secondary-ion mass spectrometry analysis (SIMS) was performed at the Woods Hole laboratory on a CAMECA IMS 3f ion probe. For analytical conditions see Webster and Duffield (1991). Volatile contents were checked by reconnaissance FTIR and Raman spectrometry at Bayerisches Geoinstitut, Bayreuth, Germany.

Geochemistry of Melt Inclusions

The alkali and silica contents (Table 3) of the melt inclusions define a rhyolitic to trachytic composition in the total alkali silica (TAS) discrimination diagram (not shown), sensu Le Bas et al. (1986). The melt inclusions of Llallagua and Cerro Rico are characterized as rhyolitic to rhyodacitic melts in the Zr/TiO_2-SiO_2 discrimination diagram (Winchester and Floyd, 1977), whereas melt inclusions of Chorolque plot in the rhyodacite and pantellerite fields, due to higher Zr concentrations (Fig. 2).

Compared to calc-alkaline bulk rock compositions, very low abundances of MgO, FeO, and CaO, and high concentrations of alkalis in the melt inclusions indicate that crystallization of quartz phenocrysts occurred after the main crystallization of mafic minerals (i.e., biotite) and plagioclase. Triangular diagrams of molar ratios of Si-Na-Ca and Si-Na-K (not shown) display constant Na/Ca ratios of the melt inclusions and are in

agreement with albite-oligoclase fractionation (Llallagua, Cerro Rico) and oligoclase-andesine fractionation (Chorolque); significant variation in the molar K/Na ratios suggests formation of alkali-feldspars synchronous with quartz crystallization.

The melt inclusions are enriched in incompatible components such as Ta (6–17 ppm), B (35–643 ppm), Cs (20–194 ppm), Rb (176–637 ppm), Li (13–623 ppm), Sn (16–43 ppm), W (5–47 ppm), and As (7–85 ppm), and are depleted in Zr (15–85 ppm) and TiO_2 (0.03–0.14 wt %) with respect to crustal averages (Figs. 4 and 5). Compared to upper crust (Taylor and McLennan, 1985), the mean compositions of the melt inclusions are up to fivefold lower in Ba, Zn, Zr, Na_2O, and CaO, more than fivefold lower in Sr, TiO_2, FeO, and MgO, and up to fivefold higher in K_2O, Rb, Pb, Ta, Hf, and Th. Strong enrichment of more than five times upper crust is seen for As, W, U, Sn, Cs, and B (Table 3).

The melt inclusion data show good correlations in log-log variation diagrams, and they align with the regional fractionation trends (Figs. 4a-e, 5a-d). Fractionation trends of Tertiary magmatic rocks of the Andean tin belt are defined by late Miocene rhyodacitic ash flow tuffs of the Los Frailes volcanic field (Dietrich, 1994), granitic intrusions of the Oligocene-early Miocene Cordillera Quimsa Cruz (Miller, 1988), the late Miocene quartz latites to rhyolites of the Morococala volcanic field (Morgan et al., 1998), and by the Macusani ash flow tuffs and obsidian glasses. The Miocene-Pliocene Macusani ash flow tuffs and quenched obsidian glasses of southern Peru represent extremely fractionated, strongly peraluminous, S-type magmatic rocks with compositions close to tin granites (Noble et al., 1984; Pichavant et al., 1987, 1988). The melt inclusion data points of the tin porphyries plot between the Macusani tuffs and Macusani obsidian glasses (Figs. 4a-e, 5a-d), and demonstrate the highly fractionated composition of the entrapped melt phase, similar to tin granites or high silica rhyolites.

Boundary-layer effects are unlikely to have controlled the systematic enrichment and depletion patterns of the melt inclusions because the inclusions are in accordance with regional fractionation trends of Tertiary felsic systems of the Andean tin belt (Figs. 4a-e, 5a-d). If boundary layer effects would have been important in the melt inclusion suite, both incompatible as well as compatible (with respect to bulk felsic systems) trace elements should be enriched in the inclusions because most trace elements behave incompatibly with respect to quartz (Nash and Crecraft, 1985). Boundary-layer effects are compositional gradients at crystal-liquid interfaces that are controlled by velocities of crystal growth, compatibility of elements to growing mineral phases, reequilibration rates of adjacent liquid, and style of chemical exchange (diffusion vs. convection; Roedder, 1979; Bacon, 1989).

High Rb/Sr ratios of 0.9 to 60 are attributed to an advanced degree of feldspar fractionation (Fig. 4c). An advanced degree of magmatic fractionation of the melt inclusions is also inferred from uncoupling of geochemically coherent element pairs (Nb/Ta <10, Zr/Hf <<16, Th/U <4), which results from enrichment in Ta, Hf, and U at relatively constant low levels of Nb, Zr, and Th (Dietrich, 1999).

Data points of the melt inclusions overlap in the log-log Nb-Ta variation diagram (Fig. 4f) with reference data of highly fractionated granitic and rhyolitic systems, such as the French Beauvoir granite (Raimbault et al., 1995), tin granites of Pilok, Thailand (Lehmann et al., 1994), the granite sequence of the German Erzgebirge (Tischendorf, 1989), and most fractionated (rhyolitic) ash flow tuffs of the Morococala volcanic field, Bolivia (Morgan et al., 1998).

Ratios of Zr/Hf of much less than 16 are far below crustal averages of 30 to 40. The majority of the melt inclusions are even below the Zr/Hf ratios of the highly fractionated Macusani tuffs or the Beauvoir rare-metal granite. The PIXE data should be correct because Zr and Hf both belong to the element suite that defines the calibration curve. Hafnium enrichment in late phases of the Beauvoir granite with Zr/Hf less than 16 was attributed to late magmatic-hydrothermal processes by Raimbault et al. (1995).

Temperature of entrapment

Zircon is an accessory component of the tin porphyry systems. Watson (1979) and Watson and Harrison (1983) found that zirconium solubility is a function of melt composition, M (the molar cation ratio, $M = (Na + K + 2Ca)/(Al \times Si)$) and temperature, T [K]:

$$\ln D_{Zr}^{zircon/melt} = \{-3.80-[0.85\,(M-1)]\} + 12900/T \qquad (1)$$

Application of this formula to Zr concentrations and molar cation ratios of melt inclusions gives temperatures of inclusion entrapment between 620° and 740°C (Fig. 6). Melt inclusions of Chorolque range in temperature between 680° and 720°C, those of Llallagua have temperatures between 650° and 740°C, and melt inclusions of Cerro Rico give temperatures between 620° and 680°C. This temperature range of melt inclusions fits well within curves of liquidus and solidus of water saturated granitic melts at ≥1 kbar (Fig. 7; Luth, 1969; Stern and Wyllie, 1973; Stern et al., 1975) and with other experimental results of natural granitic systems at low pressure-temperature conditions (Maaløe and Wyllie, 1975; Johannes and Holtz, 1996).

Volatile contents of melt inclusions

Reconnaissance ion microprobe (SIMS) analyses of eight melt inclusions give H_2O concentrations between 4.7 wt percent and 0.6 wt percent H_2O. FTIR spectrometry results range from 2.64 to 0.15 wt percent H_2O (Cerro Rico: 0.28–1.30 wt % H_2O, Llallagua: 0.55–2.64 wt % H_2O, Chorolque: 0.15–0.46 wt % H_2O). Totals of EMPA analyses of the melt inclusions (92.7–102.4 wt %) give, aside from analytical uncertainties, a rough estimate of volatile contents up to 7.3 wt percent. Neither CO_2 nor CH_4 has been detected by reconnaissance Raman spectrometry.

The wide scatter of water concentrations is attributed to partial loss of volatiles after entrapment. Loss of volatiles of the melt inclusions has been discussed in terms of diffusive escape and reequilibration of H_2 (Roedder, 1979), H_2O, OH^-, and H^+ (Qin et al., 1992), and partial decrepitation along microcracks (Roedder, 1979; Tait, 1992). Therefore, the measured volatile contents of the melt inclusions can be taken as minima of the bulk system, inferring initial water concentrations of about 5 wt percent H_2O, i.e., water-saturated conditions.

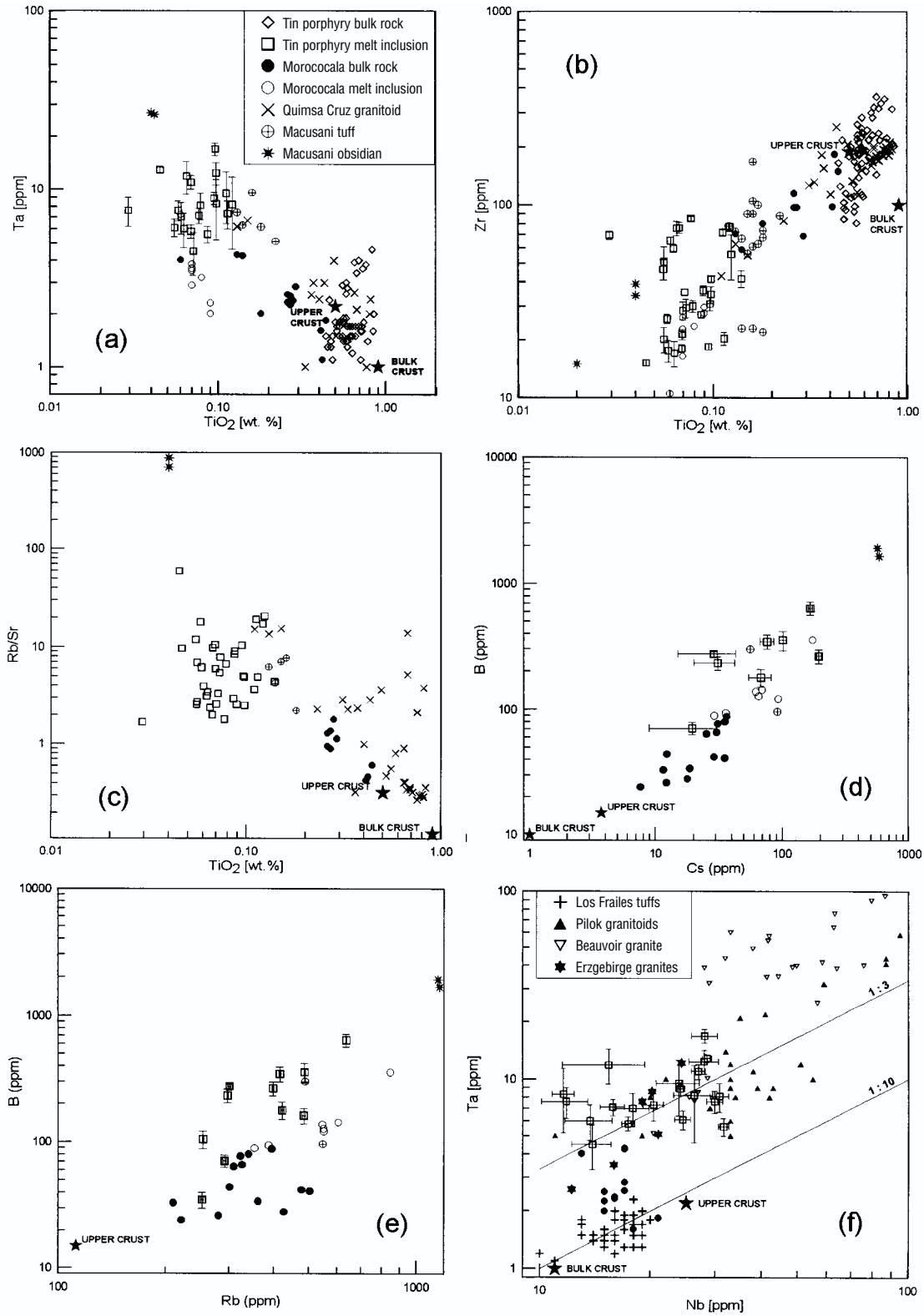

FIG. 4. Log-log variation diagrams of a. TiO_2 vs. Ta; b. TiO_2 vs. Zr; c. TiO_2 vs. Rb/Sr; d. Cs vs. B; e. Rb vs. B; and f. Nb vs. Ta for melt inclusion and bulk rock data from the Andean tin belt (Dietrich, 1999). Melt inclusion data are from Llallagua, Chorolque, and Cerro Rico (by NRA, SIMS (B, Li), and PIXE methods; error bars: 1 σ counting statistics); bulk rock data are from Llallagua, Chorolque, Oruro, and Cerro Rico. Reference data of the Morococala volcanic field (Morgan et al., 1998), Quimsa Cruz granitoids (Miller, 1988), Macusani volcanic rocks (Noble et al., 1984; Pichavant et al., 1987, 1988), Los Frailes tuffs (Dietrich, 1994), Pilok tin granites (Lehmann et al., 1994), Beauvoir rare-metal granite (Raimbault et al., 1995), Erzgebirge granite suite (Tischendorf, 1989), and bulk and upper crust (Taylor and McLennan, 1985) are shown.

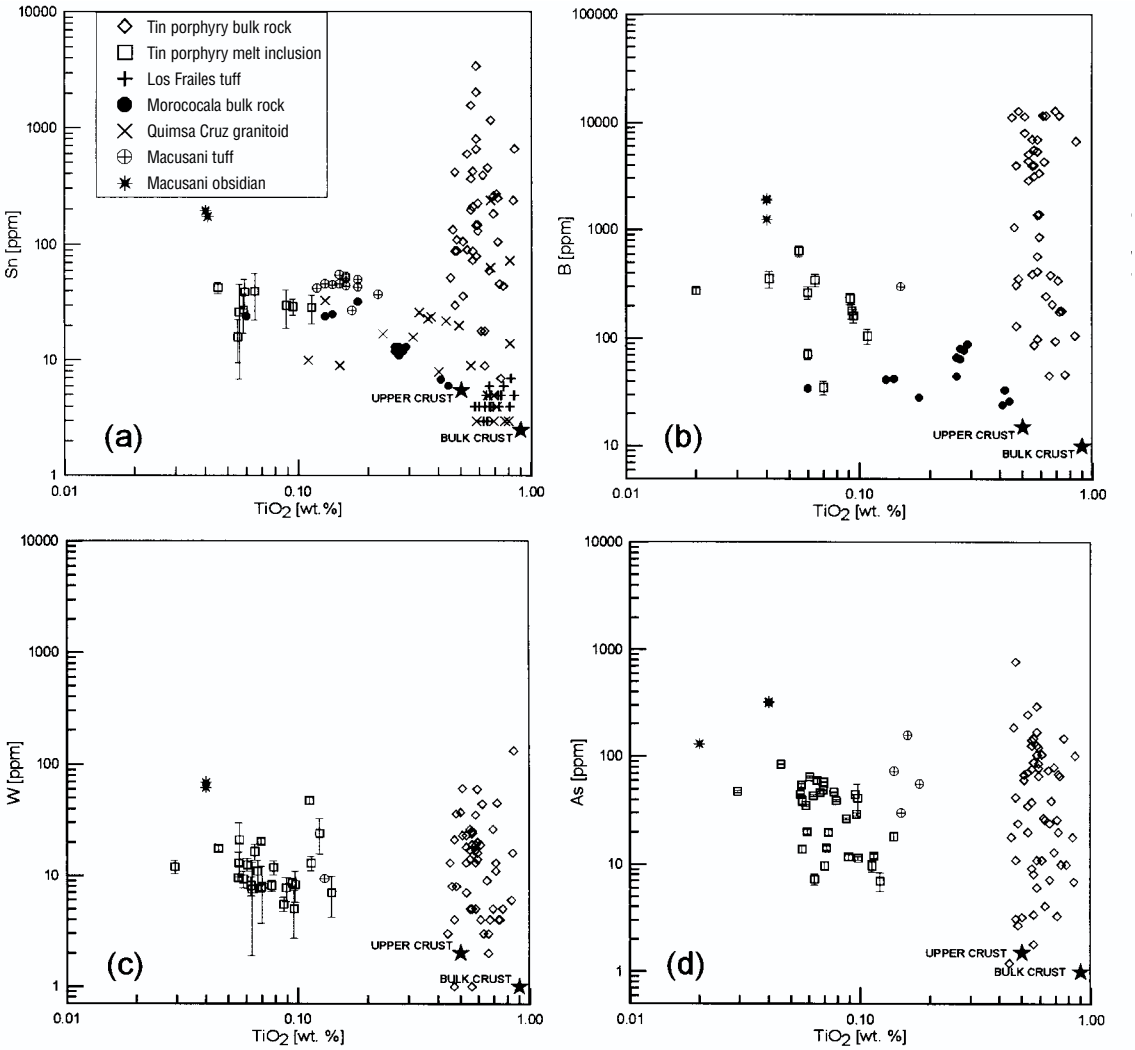

FIG. 5. Log-log variation diagrams of a. TiO_2 vs. Sn; b. TiO_2 vs. B; c. TiO_2 vs. W; and d. TiO_2 vs. As. Melt inclusion data are from Llallagua, Chorolque and Cerro Rico (by NRA and SIMS (B), and PIXE; error bars: 1 σ counting statistics), bulk rock data are from Llallagua, Chorolque, Oruro, and Cerro Rico. Reference data of the Morococala volcanic field (Morgan et al., 1998), Quimsa Cruz granitoids (Miller, 1988), Macusani volcanic rocks (Noble et al., 1984; Pichavant et al., 1987, 1988), Los Frailes tuffs (Dietrich, 1994), and bulk and upper crust (Taylor and McLennan, 1985) are shown.

Primary vapor inclusions and some melt inclusions with exceptionally large vapor bubbles in quartz phenocrysts point to water saturation of the melt, with some exsolution of free vapor phases. However, simultaneous entrapment of melt and volatile phases appears unlikely to have controlled the variable water concentrations, because volume proportions of vapor bubbles are fairly constant in the analyzed melt inclusions.

The outlined crystallization sequence of plagioclase, biotite, alkali-feldspar, and quartz coexisting with liquid ± vapor, and water concentrations of about 5 wt percent H_2O, are consistent with experimental results on low-pressure, water-saturated granitic melts (Maaløe and Wyllie, 1975; Stern et al., 1975; Johannes and Holtz, 1996).

Chlorine data (EMPA and PIXE) have a log-normal distribution in the probability net (not shown). Overlapping populations of the subvolcanic systems of Llallagua and Cerro Rico have geometric means of about 1,300 ± 625 ppm Cl, while the melt inclusions of Chorolque are characterized by a higher geometric mean of 2,250 ± 625 ppm Cl. Exceptionally high Cl concentrations between 4,000 and 6,000 ppm Cl have been detected in some samples from all systems and point to distinct chloride phases within the melt inclusions (Carroll and Webster, 1994).

Fluorine concentrations are below the EMPA limits of detection of 0.15 wt percent, and distinctly lower than fluorine data from melt inclusions of tin-bearing topaz rhyolite systems in Mexico and the western United States (Webster and Duffield, 1991, 1994; Webster et al., 1996). The bulk rock data of the Bolivian tin porphyry systems are relatively low in fluorine as well (700–2,700 ppm F).

Sulfur concentrations of the melt inclusions (PIXE) range from less than 40 to 207 ppm S and show a log-normal distribution with a geometric mean of 25 ppm S for all systems (probability net not shown). Low sulfur concentrations of the

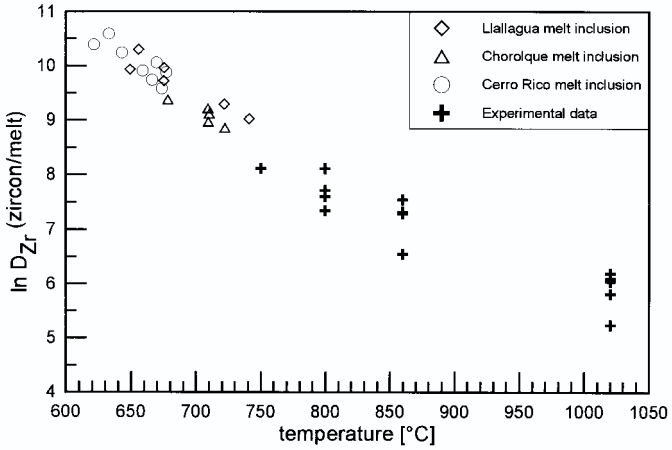

FIG. 6. Variation diagram of temperature vs. $\ln D_{Zr}$ (zircon/melt) for melt inclusions and experimental data from Watson and Harrison (1983).

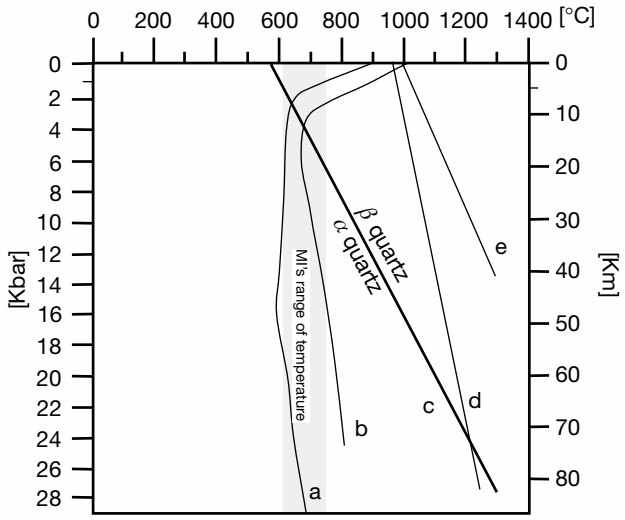

FIG. 7. Range of entrapment temperatures of melt inclusions (MI) deduced from Zr concentrations (shaded field) compared to experimental liquidus and solidus curves, a, solidus, and b, liquidus of H_2O-saturated granitic melts (Stern et al., 1975), c, α- and β-quartz transition, and d, solidus and e, liquidus of dry granitic melts (Luth, 1969; Stern and Wyllie, 1973).

melt inclusions below 200 ppm S are consistent with the low oxidation state of ilmenite-series granitoids (Ishihara, 1981; Takagi and Tsukimura, 1997).

Discussion

Bulk rock vs. melt inclusion geochemistry

The comparison of melt inclusion and bulk rock data for immobile elements such as Ta, Zr, and TiO_2 shows a large compositional gap and a striking contrast in the degree of magmatic fractionation (Fig. 4a, b). The melt inclusions are strongly enriched in Ta and depleted in Zr and TiO_2 with respect to bulk rock composition. While bulk rock samples display an intermediate degree of fractionation and plot around average values of the upper continental crust, the compositions of the melt inclusions are similar to reference data of the highly evolved Macusani tuffs.

Mean concentrations of the melt inclusions are about threefold enriched in Ta compared to mean values of bulk rock samples. The maximum Ta concentrations of the inclusions are even sixfold (Llallagua), eightfold (Chorolque) and fivefold (Cerro Rico) higher in Ta. Assuming the extreme case of perfect incompatible behavior ($D_{xtls/melt} = 0$) for Ta, the application of the Rayleigh fractionation equation:

$$C_L = C_0 \times F^{(D-1)} \quad (2)$$

for closed-system crystal-liquid fractionation would require a degree of fractionation on the order of F = 0.2 (80 wt % crystals). However, phenocrysts make up about 50 vol percent of the tin porphyries and only a maximum twofold enrichment is consistent with crystal-liquid fractionation in a closed system. The variation ranges between minimum and maximum concentrations of incompatible elements in melt inclusions of individual systems also exceed enrichment factors of two (e.g., minimum-maximum factors for Cerro Rico: As, 6.1, Cs, 9.7). Thus, the magnitude of observed compositional gap and compositional variations among melt inclusions of the tin porphyry systems cannot be generated by crystal-liquid fractionation alone, but require additional processes.

Lu et al. (1992) made similar observations with quartz-hosted melt inclusions in pumice of the Bishop tuff. Variations of uranium concentrations of melt inclusions in the Bishop tuff would require crystallization of at least 33 wt percent phenocrysts during quartz formation. However, on average only 17 wt percent of phenocrysts is observed in pumice lumps. Mechanical loss of crystals from the magma prior to eruption therefore was proposed by Lu et al. (1992). Such a mechanism appears to be inappropriate in the case of the Bolivian tin porphyries because the minimum amount of 80 wt percent crystals, required by crystal-liquid fractionation, is too high for volcanic rocks.

In an attempt to link the compositions of melt inclusions with bulk rock geochemistry we consider both a closed-system and an open-system scenario: a compositionally zoned magma chamber, and mixing of two end members.

Compositionally zoned magma chamber

Compositionally zoned magma chambers are well-established features of volcanic systems. Strong variations of trace elements between members of volcanic sequences and generation of highly fractionated high-silica rhyolites have been discussed in terms of fractional crystallization, partial melting, volatile exsolution, diffusive processes, and convective fractionation (Hildreth, 1981; Mahood and Hildreth, 1983; Miller and Mittlefehldt, 1984; Sparks et al., 1984; Congdon and Nash, 1991).

We imagine a scenario of a compositionally zoned magma chamber with portions ranging from highly fractionated to intermediate. The consistently highly fractionated nature of quartz-hosted melt inclusions leads us to the assumption that rapid crystallization of quartz phenocrysts, with entrapment of the inclusions, occurred exclusively in the highly fractionated upper portions of the magma chamber. Within intermediate portions of the chamber, growth of quartz phenocrysts appears to have been slow to absent.

The surface expression of the magma chamber, i.e. volcanic activity, producing the subvolcanic bodies of the tin porphyries, was dominated by moderately fractionated portions of the magma chamber or by volcanic activity arising after collapse of the compositional zoning.

Mixing of two end members

Mixing of two independent magma batches, although difficult to prove, has been proposed as an important igneous process. Influx of primitive melts into calc-alkaline magma chambers can result in hybrid melt composition and can enhance or initiate volcanic activity by increasing gas pressure, reducing viscosity-density, and exchanging heat (Anderson, 1976; Huppert et al., 1982).

There is little physical evidence for mixing in the tin porphyry systems. However, a mixing event would be a likely process to link the compositional gap between the melt inclusion and bulk rock geochemistry. Influx of primitive melt into an evolved felsic magma chamber may generate hybrid magma, but also it may facilitate or trigger the volcanic activity of the tin porphyry systems (Dietrich et al., 1999).

Evaluation of the melt inclusion data shows that alkali feldspars (sanidine) crystallized synchronously with quartz. A sanidine concentrate (L18b) of the Llallagua porphyry has an ε_{Nd} value of –11, whereas bulk rock samples gave ε_{Nd} of approximately –9 (Table 2). Assuming that the isotopic signature has not been disturbed by hydrothermal processes, and that the neodymium isotope data of sanidine are representative of the environment of melt inclusion formation, mixing with 25 percent of a contaminant having ε_{Nd} of –5 would be required to explain the bulk ε_{Nd} value. Miocene shoshonites of the Eastern Cordillera and the Altiplano with ε_{Nd} of approximately –5 could represent such a contaminant (Redwood and Rice, 1997).

The supposed igneous end members of the mixing model, a rhyolitic melt and a more primitive contaminant, are not exposed in the tin porphyry systems itself, but they are seen in other parts of the Miocene Bolivian tin belt. More deeply eroded or locally uplifted segments of the Andean tin belt expose several outcrops of lower Miocene granitic intrusions, such as the plutons of the Cordilleras Quimsa Cruz, Illimani, Santa Vera Cruz, and Azanaques, which are locally associated with vein- and greisen-type tin mineralization. Minor mafic to intermediate volcanic centers have been described from the central and eastern Altiplano (Davidson and de Silva, 1992, 1995) and shoshonitic basic lavas are recognized in the eastern Altiplano and in the Eastern Cordillera (Redwood and Rice, 1997). These minor volcanic centers are controlled by lineaments and strike-slip faults and are evidence for mantle involvement in lower Miocene to Recent volcanism of the Bolivian tin belt.

Origin of ore-bearing fluids

The intermediate degree of fractionation of the Bolivian tin porphyry systems is an exception to the worldwide metallogenic association of tin mineralization with highly fractionated felsic systems (Lehmann, 1990). Elevated values of Sn, W, B, and As in bulk rock samples do not align with magmatic fractionation trends, but their scattered distributions reflect a hydrothermal overprint (Fig. 5a-d). In contrast, the melt inclusion data correspond to tin granitic compositions and show orthomagmatic enrichment trends of, for example, Sn, W, B, and As, i.e. those metals and volatiles that characterize the hydrothermal overprint and mineralization of the exposed tin porphyry bodies (Figs. 4d-e, 5a-d). The coincidence in chemical signature of the rhyolitic melt-inclusion system and the hydrothermal system suggests a genetic link, i.e., a source of the ore-bearing fluids from an unexposed tin granitic magma.

The large amount of metals and other elements brought into the tin porphyry systems during hydrothermal alteration and mineralization cannot have been derived from the exposed small subvolcanic stocks, but demands a much larger, more deeply seated source volume. Assuming a tin granitic melt with 20 ppm Sn (the mean of the Llallagua melt inclusions) and a final geochemical Sn accumulation in the Llallagua porphyry system of about 2 Mt Sn, a theoretical minimum magma volume of 43 km^3 is required (melt density: 2.3 g/cm^3). Given the fact that efficiency of metal extraction will be less than 100 percent, a much larger volume is likely.

Conclusions

The highly evolved nature of the quartz-hosted melt inclusions is remarkable in two ways. First, the compositional gap between melt inclusions and bulk rock samples requires a process of magma mixing, either in a zoned magma chamber or from two individual end members. Second, the trace element signature of the melt inclusions suggests the existence of unexposed, rare-element enriched melt portions which are a likely source for the Sn-W-B-As-bearing magmatic vapor phases. We propose the following scenario:

1. Emplacement of a crustal melt in upper crustal levels and establishment of compositional gradients ranging from intermediate to highly fractionated portions. Rhyolitic magma with ilmenite-series affinity is saturated in volatiles with some coexisting vapor phases and has elevated concentrations of incompatible elements (B, As, Rb, Cs, Ta, Sn, and W). Crystallization of quartz phenocrysts with entrapment of melt inclusions is apparently mainly restricted to highly fractionated portions.
2. Influx of primitive melt into the lower levels of the partly crystallized and compositionally zoned felsic system results in mixing and breakdown of the compositional zonation of main portions of the magma chamber. Hybrid, moderately fractionated melt ascends into shallowest levels of the crust and forms small subvolcanic rhyodacite bodies.
3. Decompression and concomitant crystallization of the magma chamber trigger release of Sn-W-B-As-bearing magmatic vapor phases from undisturbed granitic melt portions, possibly preserved in apical satellite intrusions. Magmatic vapor phases are channeled and focused by an existing volcanic vent structure and cause hydrothermal alteration-mineralization in subvolcanic host rocks.

Once the volcanic activity is initiated, the interplay of explosive venting, decompression, and catastrophic volatile release may establish a runaway mechanism that is able to efficiently extract volatile phases from deep portions of the magmatic system. The volcanic columns are predestined to

physically channel magmatic vapor phases, which in uppermost (sub)volcanic levels cause hydrothermal alteration and mineralization.

The genetic concept of deriving volcanic rocks and magmatic vapor phases from different portions of a compositionally zoned and partially mixed magma chamber may explain the exceptional metallogenic situation of the Bolivian tin porphyries, i.e., the tin mineralization in association with only moderately fractionated felsic host rocks.

Acknowledgments

This study was financed by Deutsche Forschungsgemeinschaft (grant Le 578/9-1). Fieldwork was supported by Servicio Geológico de Bolivia (GEOBOL-SERGEOMIN), Corporación Minera de Bolivia (COMIBOL), Cooperativa Minera Siglo XX, Cooperativa Minera Chorolque, and Empresa Minera Zumaj Orcko. ICP-MS analyses were carried out by Peter Dulski (GFZ, Potsdam), and SIMS microanalyses by Jim Webster (AMNH, New York). NRA microanalyses at Laboratoire Pierre Süe, Saclay, France were supported by Michelle Mosbah and Nicole Métrich. Neodymium isotope analysis was performed at the University of Goettingen by Jan Heinhorst, in cooperation with Prof. Brent Hansen. FTIR and Raman spectrometry at Bayerisches Geoinstitut was realized by courtesy of Hans Keppler. We thank all persons and institutions (mentioned or not) who helped to realize this study. Criticial comments by *Economic Geology* reviewers George Morgan VI and James A. Stimac helped to improve the manuscript.

December 22, 1998; September 25, 1999

REFERENCES

Ahlfeld, F., 1931, The tin ores of Uncía-Llallagua, Bolivia: Economic Geology, v. 26, p. 241–257.

——1967, Metallogenetic epochs and provinces of Bolivia: Mineralium Deposita, v. 2, p. 291–311.

Ahlfeld, F., and Schneider-Scherbina, A., 1964, Los yacimientos minerales y de hidrocarburos de Bolivia: Boletin Departamento Nacional de Geología, La Paz, v. 5, p. 1–388.

Anderson, A.T., 1976, Magma mixing: Petrological process and volcanological tool: Journal of Volcanology and Geothermal Research, v. 1, p. 3–33.

Bacon, C.R., 1989, Crystallization of accessory phases in magmas by local saturation adjacent to phenocrysts: Geochimica et Cosmochimca Acta, v. 53, p. 1055–1066.

Basu, A.R., Sharma, M., and DeCelles, P.G., 1990, Nd, Sr-isotopic provenance and trace element geochemistry of Amazonian foreland basin fluvial sands, Bolivia and Peru: Implications for ensialic Andean orogeny: Earth and Planetary Science Letters, v. 100, p. 1–17.

Carroll, M.R., and Webster, J.D., 1994, Solubilities of sulfur, noble gases, nitrogen, chlorine, and fluorine in magmas: Reviews in Mineralogy, v. 30, p. 231–279.

Congdon, R.D., and Nash, W.P., 1991, Eruptive pegmatite magma: Rhyolite of the Honeycomb Hills, Utah: American Mineralogist, v. 76, p. 1261–1278.

Cunningham, C.G., Zartman, R.E., McKee, E.H., Rye, R.O., Naeser, C.W., Sanjinés, O., Ericksen, G.E., and Tavera, F., 1996, The age and thermal history of Cerro Rico de Potosi, Bolivia: Mineralium Deposita, v. 31, p. 374–385.

Davidson, J.P., and de Silva, S.L., 1992, Volcanic rocks from the Bolivian Altiplano: Insights into crustal structure, contamination, and magma genesis in the central Andes: Geology, v. 20, p. 1127–1130.

——1995, Late Cenozoic magmatism of the Bolivian Altiplano: Contributions to Mineralogy and Petrology, v. 119, p. 387–408.

Dietrich, A., 1994, Geologie, Petrographie und Geochemie des vulkanogenen Epithermal-systems am Cerro Chakachivi, Meseta de Los Frailes/Bolivien: Unpublished diploma thesis, Clausthal-Zellerfeld, Germany, Technische Universitaet, 88 p.

——1999, Metallogenie, Geochemie und Schmelzeinschluss-Untersuchungen von tin porphyry und copper porphyry Lagerstaetten der zentralen Anden (Bolivien, Chile): Ph.D. thesis, Clausthal-Zellerfeld, Germany, Technische Universitaet: Clausthaler Geowissenschaftliche Dissertationen, v. 57, 198 p.

Dietrich, A., Lehmann, B., Wallianos, A., Traxel, K., and Palacios, C., 1999, Magma mixing in Bolivian tin porphyries: Naturwissenschaften, v. 86, p. 40–43.

Francis, P.W., Baker, M.C.W., and Halls, C., 1981, The Kari Kari caldera, Bolivia and the Cerro Rico stock: Journal of Volcanological and Geothermal Research, v. 10, p. 113–124.

Grant, J.N., Halls, C., Avila, W., and Avila, G., 1977, Igneous geology and the evolution of hydrothermal systems in some subvolcanic tin deposits of Bolivia: Geological Society of London Special Publication, v. 7, p. 117–126.

Grant, J.N., Halls, C., Avila, W., and Snelling, N.J., 1979, K-Ar Ages of igneous rocks and mineralization in part of the Bolivian tin belt: Economic Geology, v. 74, p. 838–851.

Grant, J.N., Halls, C., Sheppard, S.M.F., and Avila, W., 1980, Evolution of the porphyry tin deposits of Bolivia: Mining Geology Special Issue, Tokyo, v. 8, p. 151–173.

Hildreth, W., 1981, Gradients in silicic magma chambers: Implications for lithospheric magmatism: Journal of Geophysical Research, v. 86, p. 10153–10192.

Huppert, H.E., Sparks, R.S.J., and Turner, J.S., 1982, Effects of volatiles on mixing in calc-alkaline magma systems: Nature, v. 297, p. 554–557.

Ishihara, S., 1981, The granitoid series and mineralization: Economic Geology, 75th Anniversary Volume, p. 458–484.

Johannes, W., and Holtz, F., 1996, Petrogenesis and experimental petrology of granitic rocks: Berlin, Springer, 335 p.

Le Bas, M.J., Le Maitre, R.W., Streckeisen, A., and Zanettin, B., 1986, A chemical classification of volcanic rocks based on the total alkali-silica diagram: Journal of Petrology, v. 27, p. 745-750.

Lehmann, B., 1990, Metallogeny of tin: Berlin, Springer, 211 p.

Lehmann, B., Jungyusuk, N., Khositanont, S., Höhndorf, A., and Kuroda, Y., 1994, The tin-tungsten ore system of Pilok, Thailand: Journal of Southeast Asian Earth Sciences, v. 10, p. 51–63.

Lowenstern, J.B., 1994, Chlorine, fluid immiscibility, and degassing in peralkaline magmas from Pantelleria, Italy: American Mineralogist, v. 79, p. 353–369.

——1995, Applications of silica-melt inclusions to the study of magmatic volatiles: Mineralogical Association of Canada Short Course, v. 23, p. 71–99.

Lu, F., Anderson, A.T., and Davis, A.M., 1992, Melt inclusions and crystal-liquid separation in rhyolitic magmas of the Bishop tuff: Contributions to Mineralogy and Petrology, v. 110, p. 113–120.

Ludwig, K.R., 1993, ISOPLOT—a plotting and regression program for radiogenic-isotope data, version 2.70: U.S. Geological Survey Open File Report 91-445, 42 p.

Luth, W.C., 1969, The system $NaAlSi_3O_8$-SiO_2 and $KAlSi_3O_8$-SiO_2 to 20 kb and the relationship between H_2O content, P_{H_2O}, and P_{total} in granitic magmas: American Journal of Science, v. 267A, p. 325–341.

Maaløe, S., and Wyllie, P.J., 1975, Water content of a granitic magma deduced from the sequence of crystallization determined experimentally with water-undersaturated conditions: Contributions to Mineralogy and Petrology, v. 52, p. 175–191.

Mahood, G., and Hildreth, W., 1983, Large partition coefficients for trace elements in high-silica rhyolites: Geochimica et Cosmochimica Acta, v. 47, p. 11–30.

Maxwell, J.A., Campbell, J.L., and Teesdale, W.J., 1989, The Guelph software package: Nuclear Instruments and Methods in Physics Research, v. B43, p. 218–230.

Maxwell, J.A., Teesdale, W.J., and Campbell, J.L., 1995, The Guelph software package II: Nuclear Instruments and Methods in Physics Research, v. B95, p. 407–421.

McBride, S.L., Robertson, C.R.R., Clark, A.H., and Farrar, E., 1983, Magmatic and metallogenetic episodes in the northern tin belt, Cordillera Real, Bolivia: Geologische Rundschau, v. 72, p. 685–713.

Miller, J.F., 1988, Granite petrogenesis in the Cordillera Real, Bolivia and crustal evlution in the central Andes: Unpublished Ph.D. thesis, Milton Keynes, Open University, 198 p.

Miller, J.F., and Harris, N.B.W., 1989, Evolution of continental crust in the central Andes: Constraints from Nd isotope systematics: Geology, v. 17, p. 615–617.

Miller, C.F., and Mittlefehldt, D.W., 1984, Extreme fractionation in felsic magma chambers: A product of liquid-state diffusion or fractional crystallization?: Earth and Planetary Science Letters, v. 68, p. 151–158.

Morgan, G.B., and London, D., 1996, Optimizing the electron microprobe analysis of hydrous alkali alumosilicate glasses: American Mineralogist, v. 81, p. 1176–1185.

Morgan, G.B., London, D., and Luedke, R.G., 1998, Petrochemistry of late Miocene peraluminous silicic volcanic rocks from the Morococala field, Bolivia: Journal of Petrology, v. 39, p. 601–632.

Mosbah, M., Clochiatti, R., Métrich, N., Piccot, D., Rio, S., and Tirira, J., 1995, The characterization of glass inclusions through nuclear microprobe: Nuclear Instruments and Methods in Physics Research, v. B104, p. 271–275.

Nash, W.P., 1992, Analysis of oxygen with the electron microprobe: Applications to hydrated glass and minerals: American Mineralogist, v. 77, p. 453–457.

Nash, W.P., and Crecraft, H.R., 1985, Partition coefficients for trace elements in silicic magmas: Geochimica et Cosmochimica Acta, v. 49, p. 2309–2322.

Nielsen, C.N., and Sigurdsson, H., 1981, Quantitative methods for electron microprobe analysis of sodium in natural and synthetic glasses: American Mineralogist, v. 66, p. 547–552.

Noble, D.C., Vogel, T.A., Peterson, P.S., Landis, G.P., Grant, N.K., Jezek, P.A., and McKee, E.H., 1984, Rare-element-enriched, S-type ash flow tuffs containing phenocrysts of muscovite, southeastern Peru: Geology, v. 12, p. 35–39.

Pichavant, M., Herrera, J.V., Boulmier, S., Brique, L., Joron, J.-L., Juteau, M., Marin, L., Michard, A., Sheppard, S.M.F., Treuil, M., and Vernet, M., 1987, The Macusani glasses, SE Peru: Evidence of chemical fractionation in peraluminous magmas: Geochemical Society Special Publications, v. 1, p. 359–373.

Pichavant, M., Kontak, D.J., Brique, L., Herrera, J.V., and Clark, A.H., 1988, The Miocene-Pliocene Macusani volcanics, SE Peru: Contributions to Mineralogy and Petrology, v. 100, p. 300–338.

Qin, Z., Lu, F., and Anderson, A.T., Jr., 1992, Diffusive reequilibration of melt and fluid inclusions: American Mineralogist, v. 77, p. 565–576.

Raimbault, L., Cuney, M., Azenott, C., Duthou, J.L., and Joron, J.L., 1995, Geochemical evidence for a multistage magmatic genesis of Ta-Sn-Li mineralization in the granite at Beauvoir, French Massif Central: Economic Geology, v. 90, p. 548–576.

Redwood, S.D., and Rice, C.M., 1997, Petrogenesis of Miocene basic shoshonitic lavas in the Bolivian Andes and implications for hydrothermal gold, silver and tin deposits: Journal of South American Earth Sciences, v. 10, p. 203–221.

Rio, S., Métrich, N., Mosbah, M., and Massiot, P., 1995, Lithium, boron and beryllium in volcanic glasses and minerals studied by nuclear microprobe: Nuclear Instruments and Methods in Physics Research, v. B100, p. 141–148.

Rivas, S., and Carrasco, R., 1968, Geología y yacimientos minerales de la región de Potosí: Boletin GEOBOL, v. 11, 95 p.

Roedder, E., 1979, Origin and significance of magmatic inclusions: Bulletin Minéralogie [Paris], v. 102, p. 487-510.

——1984, Fluid inclusions: Reviews in mineralogy of the Mineralogical Society of America, v. 12, 644 p.

Samoyloff, V., 1934, The Llallagua-Uncía tin deposit: Economic Geology, v. 29, p. 481–499.

Schneider, A., 1985, Eruptive processes, mineralisation and isotopic evolution of the Los Frailes-Kari Kari Region/Bolivia: Unpublished Ph.D. thesis, London, University of London, 280 p.

Sillitoe, R.H., Halls, C., and Grant, J.N., 1975, Porphyry tin deposits in Bolivia: Economic Geology, v. 70, p. 913–927.

Sillitoe, R.H., Steele, G.B., and Thompson, J.F.H., 1998, Advanced argillic lithocaps in the Bolivian tin-silver belt: Mineralium Deposita, v. 33, p. 539–546.

Sparks, R.S.J., Huppert, H.E., and Turner, J.S., 1984, The fluid dynamics of evolving magma chambers: Philosophical Transactions of the Royal Society of London, v. A310, p. 511–534.

Steele, G., 1996, Metallogenesis and hydrothermal alteration at Cerro Rico, Bolivia: Unpublished Ph.D. thesis, Aberdeen, University of Aberdeen, 435 p.

Stern, C.R., and Wyllie, P.J., 1973, Water-saturated and undersaturated melting relations of a granite to 35 kilobars: Earth and Planetary Science Letters, v. 18, p. 163–167.

Stern, C.R., Huang, W.L., and Wyllie, P.J., 1975, Basalt-andesite-rhyolite-H_2O: Crystallization intervals with excess H_2O and H_2O-undersaturated liquidus surfaces to 35 kilobars, with implications for magma genesis: Earth and Planetary Science Letters, v. 28, p. 189–196.

Stimac, J.A., and Pearce, T.H., 1992, Textural evidence of mafic-felsic magma interaction in dacite lavas, Clear Lake, California: American Mineralogist, v. 77, p. 795–809.

Sugaki, A., Ueno, H., Kitakaze, A., Hayashi, K., Kojima, S., Shimada, N., Kusachi, I., Sanjines, O., Velarde, O.J., and Sanchez, A.C., 1985, Geological and mineralogical studies on the polymetallic hydrothermal ore deposits in Andes area of Bolivia: Japan, Sendai, 338 p.

Tait, S., 1992, Selective preservation of melt inclusions in igneous phenocrysts: American Mineralogist, v. 77, p. 146–155.

Takagi, T., and Tsukumura, K., 1997, Genesis of oxidized- and reduced-type granite: Economic Geology, v. 92, p. 81–86.

Taylor, S.R., and McLennan, S.M., 1985, The continental crust: Its composition and evolution: Oxford, Blackwell, 312 p.

Tischendorf, G., 1989, Silicic magmatism and metallogenesis of the Erzgebirge: Veroeffentlichungen des Zentralinstitutes der Physik der Erde, v. 107, 316 p.

Traxel, K., Arndt, P., Bohsung, J., Braun-Dullaeus, K.-U., Maetz, M., Reimold, D., Schiebler, H., and Wallianos, A., 1995, The new Heidelberg proton microprobe: The success of a minimal concept: Nuclear Instruments and Methods in Physics Research, v. B104, p. 19–25.

Turneaure, F.S., 1935, The tin deposits of Llallagua, Bolivia: Economic Geology, v. 30, p.14–60, 170–190.

——1960, A comparative study of major ore deposits of central Bolivia: Economic Geology, v. 55, p. 217-254, 574–606.

——1971, The Bolivian tin-silver province: Economic Geology, v. 66, p. 215–225.

Wallianos, A., 1998, Mikroanalytik an magmatischen Schmelzeinschluessen und spezielle Probleme bei der Datenauswertung von PIXE-Spektren: Unpublished Ph.D. thesis, Heidelberg, Universitaet Heidelberg, 125 p.

Watson, E.B., 1979, Zircon saturation in felsic liquids: Experimental results and applications to trace element geochemistry: Contributions to Mineralogy and Petrology, v. 70, p. 407–419.

Watson, E.B., and Harrison, T.M., 1983, Zircon saturation revisited: Temperature and composition effects in a variety of crustal magma types: Earth and Planetary Science Letters, v. 64, p. 295–304.

Webster, J.D., and Duffield, W.A., 1991, Volatiles and lithophile elements in Taylor Creek rhyolite: Constraints from glass inclusion analyses: American Mineralogist, v. 76, p. 1628–1645.

Webster, J.D., and Duffield, W.A., 1994, Extreme halogen abundances in tin-rich magma of the Taylor Creek rhyolite, New Mexico: Economic Geology, v. 89, p. 840–850.

Webster, J.D., Burt, D.M., and Aguillon, R.A., 1996, Volatile and lithophile trace-element geochemistry of Mexican tin rhyolite magmas deduced from melt inclusions: Geochimica et Cosmochimica Acta, v. 60, p. 3267–3283.

Winchester, J.A., and Floyd, P.A., 1977, Geochemical discrimination of different magma series and their differentiation products using immobile elements: Chemical Geology, v. 20, p. 325–343.

Wolf, M., 1973, Zum Magmatismus der Cordillera de Potosi in Bolivien: Leipzig, Freiberger Forschungshefte, v. C275, 174 p.

Zartman, R.E., and Cunningham, C.G., 1995, U-Th-Pb zircon dating of the 13.8 Ma dacite volcanic dome at Cerro Rico de Potosí, Bolivia: Earth and Planetary Science Letters, v. 133, p. 227–237.